

LABORATORY INVESTIGATIONS OF THE BENDING RHEOLOGY OF FLOATING SALINE ICE AND WAVE DAMPING IN THE HSVA ICE TANK

Aleksey Marchenko (1), Andrea Haase (2), Atle Jensen (3), Benjamin Lishman (4), Jean Rabault (5), Karl-Ulrich Evers (6), Mark Shortt (7), Torsten Thiel (8)









- (1) The University Centre in Svalbard, Aleksey Marchenko, Norway, E-mail: Aleksey.Marchenko@unis.no
- (2) Hamburg Ship Model Basin, Andrea Haase, Germany, E-mail: Haase@hsva.de
- (3) University of Oslo, Atle Jensen, Norway, E-mail: Atlej@math.uio.no
- (4) London South Bank University, Benjamin Lishman, UK, E-mail: Ben.Lishman@lsbu.ac.uk
- (5) University of Oslo, Jean Rabault, Norway, E-mail: Jean.Rblt@gmail.com
- (6) Solutions4arctic, Karl-Ulrich Evers, Germany, E-Mail: kueham@gmail.com
- (7) University College London, Mark Shortt, UK, E-mail: Mark.Shortt.12@ucl.ac.uk
- (8) Advanced Optics Solutions GmbH, Torsten Thiel, Germany, E-mail: thiel@aos-fiber.com

An experiment on the propagation of flexural-gravity waves was performed in the HSVA ice tank. Physical characteristics of the water-ice system were measured in different locations in the tank during the tests, with a number of sensors deployed in the water, on the ice and in the air. Water velocity was measured with an acoustic doppler velocimeter (ADV) and an acoustic doppler current profiler (ADCP); wave amplitudes were measured with ultrasonic sensors and the optical system Qualisys; in-plane deformations of the ice and the temperature of the ice and water were measured by fiber optic sensors, and acoustic emissions were recorded with compressional crystal sensors. All together 61 tests were performed, with ice thicknesses of 3 cm and 5 cm. The experimental setup and selected results of the tests are discussed in this paper. We show that the formation of cracks in the ice, caused by the action of waves, increases wave damping.

1. ORGANIZING OF EXPERIMENT

The experimental programme was focused on the investigation of surface wave propagation below solid ice. Therefore, 38 tests were performed with solid ice, 1 test with the ice split into square blocks manually, and 2 tests with the ice broken by waves. Two groups of tests (TGI and TGII) were conducted during the test programme. The ice thickness was 3 cm in TGI and 5 cm in TGII. Measurements were performed with the sensors listed in Table 1. A Qualisys™ motion capture system is used to detect the rigid body motions of the ice in all six degrees of freedom (6-DOF). The system uses four cameras, installed on the main carriage, to detect markers which are located at different positions on the model. In this paper only experiments of TGII are considered. Locations of the installed sensors are shown in Fig. 1.

Table 1. List of sensors, their short names and symbols.

Sensors (Full names)	Abbreviated name	No. of sensors	Symbol in Fig.1
Acoustic Doppler Current Profiler	ADCP	3	
Acoustic Doppler Velocimeter	ADV	2	
Acoustic Emission Transducers	AE	8	
Fiber Bragg Grating Strain Sensors	FBGS	8	
Fiber Bragg Grating Thermistor String	FBRGT	2	
Qualisys™	Q	6	
Ultrasonic sensors	US	24	
Water pressure sensor	WP	8	

TGI and TGII included similar tests performed with varying wave frequencies in the range from 0.7 Hz to 1 Hz and varying open water wave heights in the range from 0.5 cm to 1.5 cm. These

tests were repeated on (a) steady ice and (b) ice cyclically moving along the x-direction with an amplitude of about 1 m. Cyclic motion of the ice was produced manually by two persons pushing and pulling the entire ice sheet along the tank using two poles with hooks. TGI finished with tests performed on manually broken ice with rectangular floes (1.8x1.8 m). TGII finished with tests on the ice after it had been broken by waves.

The model ice cover has salinity of 2.8-3.2ppt and consists of two layers. During the experiment campaign from 15 January to 18 January 2018 the salt content in the ice decreased from about 3.2ppt to 1.6ppt due to drainage of brine. The upper layer, of about 5 mm thickness, consisted of granular crystals as a result of the seeding process. The average grain diameter is about 1 mm. Thereafter, the ice continues to grow, forming relatively long columnar crystals. These crystals reach a diameter of about 2-4 mm at the bottom of the 50 mm thick ice sheet. Air is pumped into the water during the ice growth, such that micro air bubbles of 200-500µm diameter are trapped by the ice crystals and are distributed homogeneously in the ice cover.

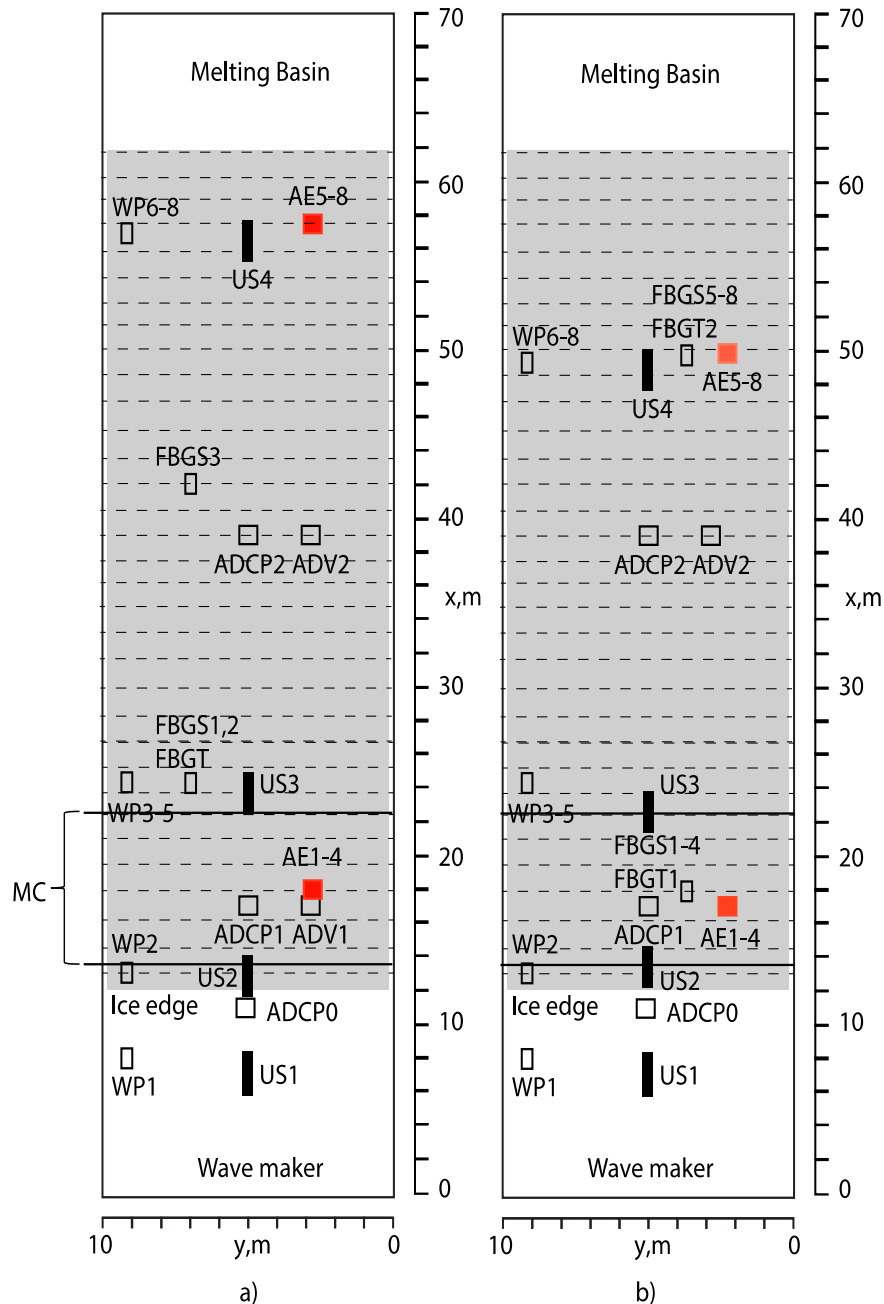


Figure 1. Locations of the sensors in TGI (a) and TGII (b). Designations are given in Table 1.

The elastic modulus and flexural strength of model ice was measured each day using a point loading method and flexural strength tests with floating cantilever beams. The mean values of the

elastic modulus and flexural strength measured in TGI and TGII are shown in Table 2. 'AT' and 'BT' denote values measured before and after the tests. There is a reduction of flexural strength during TGII.

Table 2. Elastic moduli and flexural strengths measured during TGI and TGII

TGI		TGII			
E, MPa	σ_f , kPa	E, MPa (BT)	E, MPa (AT)	σ_f , kPa (BT)	σ_f , kPa (AT)
43	92	250	245	118	86

These wave heights were programmed before the wave maker starts to work. The ice sheet affects actual wave heights in the tank due to damping in the ice covered region ($8 \text{ m} < x < 62 \text{ m}$) and due to reflections from the ice edge in the region with open water ($0 < x < 8 \text{ m}$). Wave reflection from the end of the tank can be ignored in the tests because of the small wave amplitudes at the end of the tank and the relatively small wave lengths.

2. SIMILARITY CRITERIA AND SCALING

Scaling laws for model tests with waves in ice are formulated in order to interpret the test results. Specifically, this helps to clarify which naturally-occurring wave-ice interactions are comparable to those in the tests described in this paper. In addition to the Froude ($Fr = V/\sqrt{gh}$) and Cauchy ($Ch = \rho_w V^2/E$) numbers, and wave slope (ak) used for the scaling of water-ship interaction, a set of dimensionless parameters includes

$$\rho_i/\rho_w, \nu V/gh^2, \sigma_f/\rho_w gh, E/\sigma_f, \kappa V/\nu h, \quad (1)$$

where ρ_i and ρ_w are the water and the ice densities, a and k are the amplitude and wave number, ν is the kinematic viscosity of water below the ice, V is either phase or group wave velocity, g is the acceleration due to gravity, h is the ice thickness, E is the effective elastic modulus of ice, σ_f is ice flexural strength, and κ is the permeability of ice. For broken ice, the ratio l_f/h , where l_f is a representative diameter of floes, should be added as geometrical scaling parameter. Another geometrical parameter, h/H , is added when the water depth H influences wave properties. Additional parameters proportional to rheological constants should be added to set (1) when the influence of viscous and anelastic properties of ice is important. In the experiments where the ice doesn't fail, the use of the dimensionless parameters which include flexural strength is not necessary.

The dispersion equation describing flexural-gravity waves, ignoring ice inertia, has the form

$$\omega^2 = gk \tanh(kH)(1 + Dk^4), \quad D = \frac{Eh^3}{12(1-\nu_p^2)\rho_w g}, \quad (2)$$

where ν_p is the Poisson's ratio, which for sea ice is typically between 0.3 and 0.4 (see, e.g., Timco and Weeks, 2010). For the estimates, here it is assumed that $1 - \nu_p^2 \approx 1$. Equation (2) gives the dispersion equation of gravity waves when $D = 0$. Dispersion curves of flexural-gravity waves (FGW1 and FGW2) and gravity waves (GW) are shown in Fig. 2. Curves FGW1 and FGW2 are calculated with minimum ($E = 43 \text{ MPa}$, $h = 3 \text{ cm}$) and maximum ($E = 250 \text{ MPa}$, $h = 5 \text{ cm}$) values of the elastic modulus and ice thickness measured during the tests, and a water depth of $H = 2.5 \text{ m}$, equal to the water depth in HSVA tank. The gray rectangle shows the region where most of the tests were performed. Figure 3 shows that ice elasticity is not important for wave dispersion with 3cm thick ice when the wave frequency is smaller than 0.7 Hz. The deep-water approximation is valid throughout, since $kH > 2.5$ inside the gray region in Fig. 2.

Further, the phase velocity of gravity waves in deep water is used for the calculation of $V = g/\omega$, where ω is the wave frequency in rad/s, in formula (1). The Froude number, calculated with the formula $Fr = \omega^{-1}\sqrt{g/h}$, changes from 2.2 to 5.7 in the tests described here. From dispersion equation (1) it follows that the number Dk^4 gives an estimate of the influence of elasticity on wave dispersion (instead of the Cauchy number). We consider the range of wave frequencies where $Dk^4 \approx 1$ (i.e. wave lengths are not very short) so that we can ignore the influence of the gravity

force. Expressing the wave number from the dispersion equation for gravity waves in the deep-water approximation ($\omega^2 = gk$) we find that the number $\alpha_{fg} = Eh^3\omega^8/(12\rho_w g^5)$ can be used instead of Dk^4 . Numerical values of the dimensionless coefficients E/σ_f and α_{fg} are shown in Table 3 for the ice characteristics in TGI and TGII.

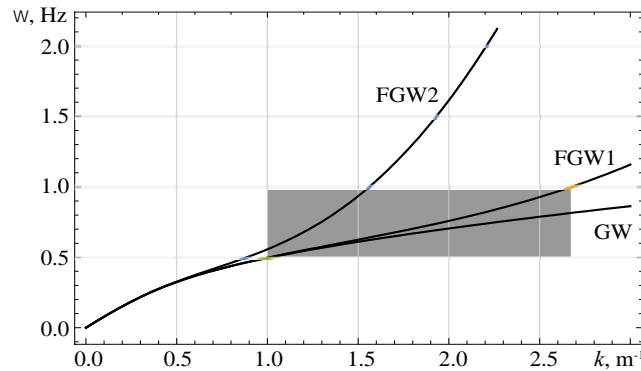


Figure 2. Dispersion equations of flexural gravity waves (FGW1,2) and gravity waves (GW).

Table 3. Dimensionless numbers characterizing the bending failure of ice and the influence of elasticity on wave dispersion in TGI and TGII.

	TGI	TGII	
$E/\sigma_f \cdot 10^{-3}$	0.47	2.1	2.8
α_{fg}	0.01-2.6	0.27-70	0.26-68

The effective elastic modulus of sea ice measured in full-scale tests with cantilever beams is $E \approx 3$ GPa and flexural strength is $\sigma_f \approx 0.3$ MPa (Marchenko et al, 2017). The ratio $E/\sigma_f \cdot 10^{-3} \approx 10$ is higher in full scale tests than it was TGI and TGII. Figure 3 shows dimensionless numbers Fr and α_{fg} calculated with the characteristics of natural sea ice and natural wind waves and swell. One can see that similarity by Froude number (2.2-5.7 in our tests) can be reached for wind waves with frequency 0.2 Hz (5 s period), swell or local waves with frequency 0.1 Hz (10 s period) in relatively thick ice ($h > 1$ m), and almost reached for low frequency swell in thick ice (30 s period and 0.033 Hz frequency). Similarity by α_{fg} (0.01-70 in our tests) can be reached only for waves with frequencies close to or higher than 0.1 Hz (10 s period) propagating in relatively thick ice. The ratio ρ_i/ρ_w is similar for the model and natural ice. Similarity by the number $\alpha_{sh} = \sigma_f/\rho_w gh$, characterizing the influence of hydrostatic pressure on bending failure, is not fulfilled, since $\sigma_f/\sigma_{f,exp} \approx 3$, while $h/h_{exp} > 10$.

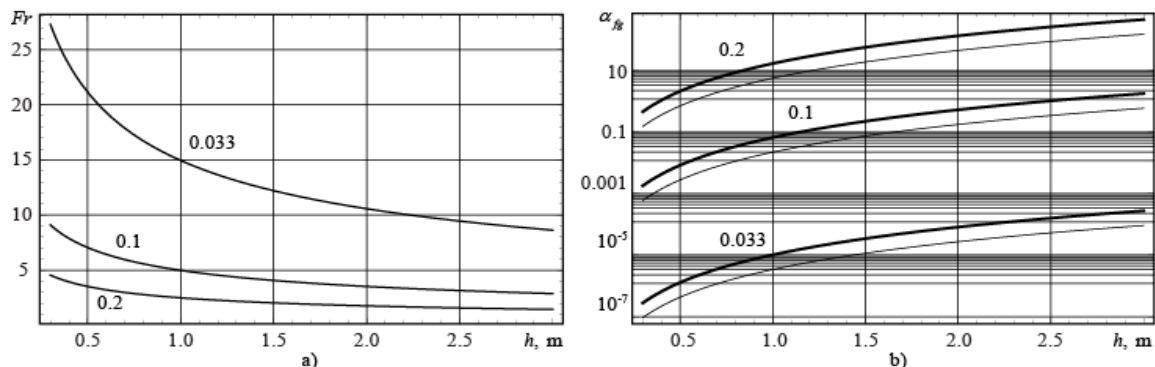


Figure 3. Dimensionless numbers Fr (a) and α_{fg} (b) versus ice thickness, calculated with the characteristics of natural sea ice. Wave frequency (Hz) is marked on the individual curves. Thick and thin lines in (b) are constructed with $E = 3$ GPa and $E = 1$ GPa respectively.

The amplitude of the wave-induced velocity of surface water particles, calculated with standard formulae following from the potential theory of surface waves with small amplitude, equals ωa . The wave amplitudes varied within 0.5 – 1.5 cm, and the wave frequencies varied within 0.5-6

rad/s in the experiment. Therefore, the velocity amplitude is estimated as varying from 1.5 cm/s to 10 cm/s in the tests. At full scale, the velocity amplitude is estimated in the same range when the wave frequency is of about 0.6 rad/s and wave amplitude is of about 10 cm. The decay distance of wave induced motion in the vertical direction is given by k^{-1} . According to Fig. 3, this decay distance extends below the ice by 0.4-1 m in the experiment, which excludes any influence of the tank bottom on the waves.

3. INSTALLATION OF FBG SENSORS

The FBG sensors were used in the experiments to measure in-plane strains in the ice (excited during propagation of surface gravity waves below the ice) and to record a vertical profile of the temperature (in the water layer below the ice, in the ice and above the ice) over a distance of 12 cm (with spatial resolution of 1 cm). A schematic of the installation of the strain and temperature sensors is shown in Fig. 4a. Each strain sensor (FBGS sensor) measures strain (FBG strain) between two points where the fiber is fixed to bolts, which in turn connect the working length of the fiber (including the FBGS sensor) to the fiber which transmits optical signal. The bolts are fixed onto brackets with nuts and washers, and each bracket is mounted on the ice with four screws. It is evident that FBG strain consists of a sum of the in-plane strain in the ice and the strain due to the bracket tilts caused by ice bending. Four FBGS sensors were deployed to measure longitudinal (x-direction) strains in the ice at distances (x-direction) of 19 m (2 sensors) and 50 m (2 sensors) from the ice edge. Another four FBGS sensors measured strains in the transversal direction to the tank axis (y-direction) in similar locations. Two FBG temperature strings (FBGT sensors) were supported by foam plastic holders so that 3 thermistors were above the ice surface. These FBGT sensors were then placed inside holes of 2 mm diameter drilled through the ice. The diameter of FBGT sensors is slightly smaller than 2 mm. Therefore, FBGT sensors were tightly held inside the holes without visible gaps. Photographs of the sensors, installed in position, are shown in Fig. 5. Measurements of strain and temperature were recorded at a frequency of 40 Hz. Strain records show a periodic dependence on time, with a dominant period equal to the wave period.

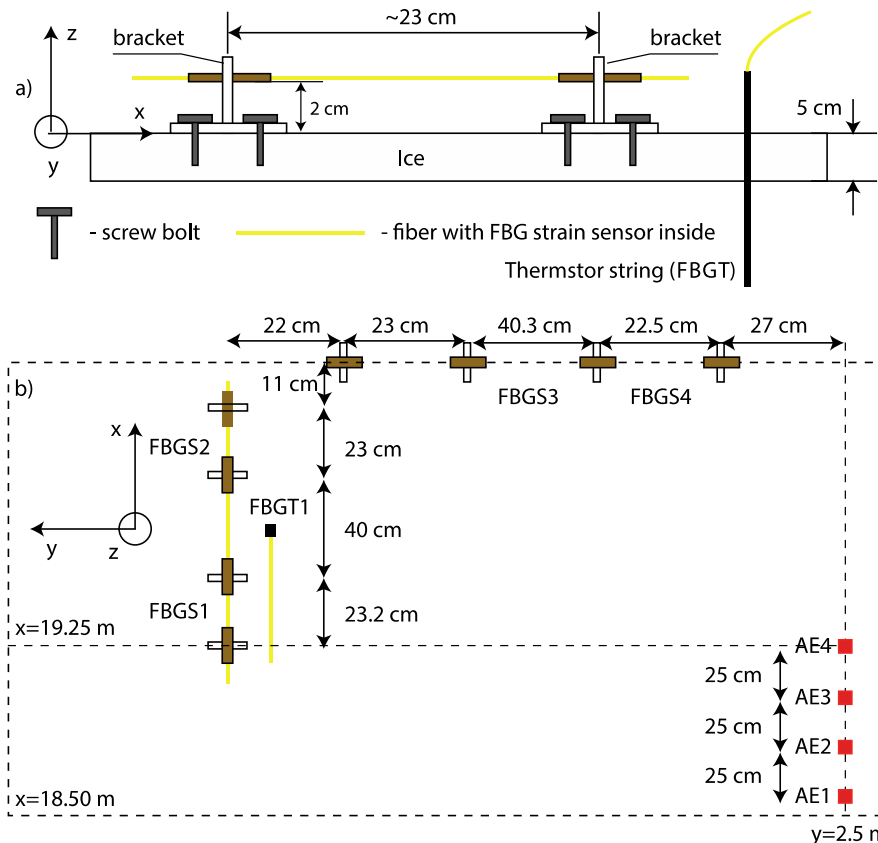


Figure 4. Scheme of the installation of FBG sensors on the ice by $x < 20$ m.

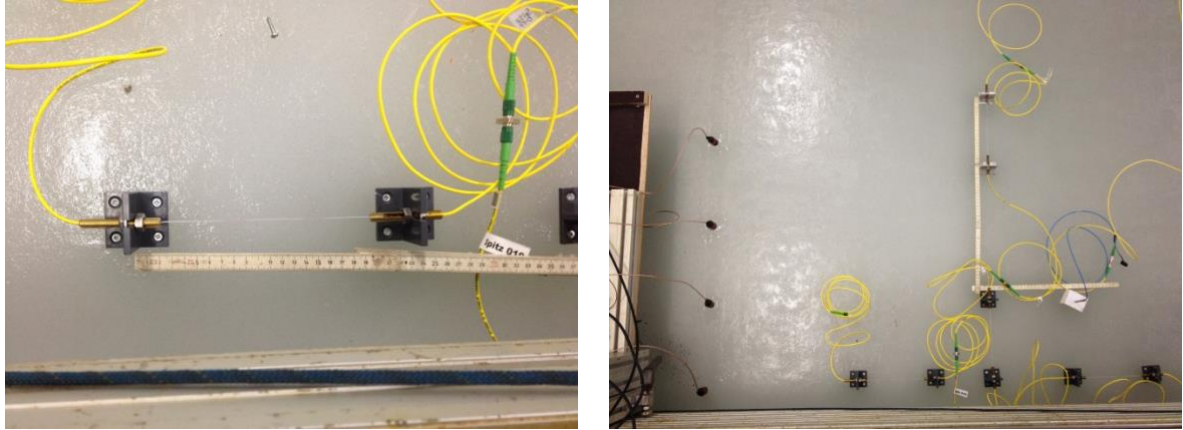


Figure 5. Mounting of FBG strain sensor on the ice (a). Four FBG strain sensors (FBGS) and thermistor string (FBGT) mounted on the ice near AE sensors (b).

4. WAVE DISPERSION AND ELASTIC MODULUS

Data analysis of sensors FBGS1 and FBGS2 (Fig. 4b) was performed to calculate wave speeds and elastic modulus of ice. Longitudinal deformation $\epsilon = \Delta L/L$, where $L = 23$ cm (Fig. 4a), measured by FBGS sensor is calculated by the formula

$$\frac{\Delta\lambda}{\lambda} = GF \cdot \epsilon, \quad (3)$$

where the variation of the peak wavelength $\Delta\lambda$ is measured with a spectrometer that receives the reflected signal from the FBGS sensor, and $GF = 0.719$ is the gauge factor obtained from a calibration cycle for the FBGS sensors in standard SMF fiber. Influence of the air temperature of the strain is ignored because the temperature changes during one tests are assumed to be small.

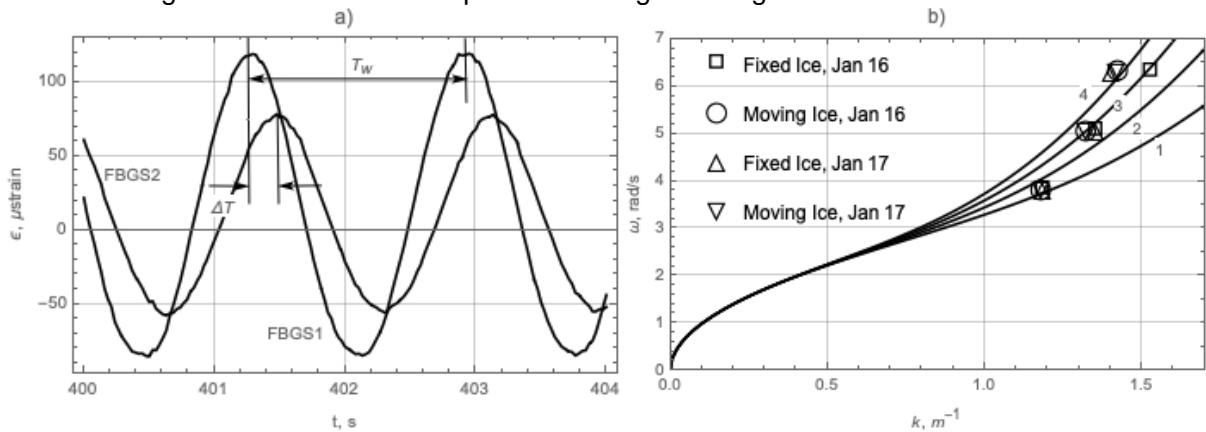


Figure 6. Example of the records of FBGS1 and FBGS2 sensors (a). Waves frequencies versus wave numbers calculated from the experiment TGII. Dispersion curves 1, 2, 3, and 4 are constructed with elastic moduli of 100, 200, 300 and 400 MPa respectively.

Figure 6a shows an example of the records of FBGS1 and FBGS2 sensors versus the time. Both of the signal show periodic dependence from the time and their period T_w coincides with the period of waves made by the wave maker. Distance between the brackets used for the mounting of the FBGS sensors is $l = 63.2$ cm. Each wave crest runs this distance during the time ΔT , therefore,

$$\frac{\omega}{k} = \frac{l}{\Delta T}. \quad (4)$$

From dispersion equation (2) written in deep water approximation ($kH \rightarrow \infty$) it follows

$$E = \frac{12\rho_w(1-\nu_p^2)\omega^2 - gk}{h^3 k^5}. \tag{5}$$

It is assumed $1 - \nu_p^2 \approx 1$ since typical value of the Poisson's ratio for ice is about 0.33. The water density is assumed equal to $\rho_w = 1000 \text{ kg/m}^3$. Formulas (4) and (5) are used to calculate wave number k and elastic modulus E from the experimental data. Values of ΔT were calculated for each period of the FBGS1 and FBGS2 records in 6 tests with fixed ice and 6 tests with moving ice with wave frequencies of 0.6 Hz, 0.8 Hz and 1.0 Hz. The tests were performed on January 16 and 17 within TGII ($h = 5 \text{ cm}$). Then, the mean values of ΔT averaged over 250 s interval were used to calculate k and E from formulas (4) and (5).

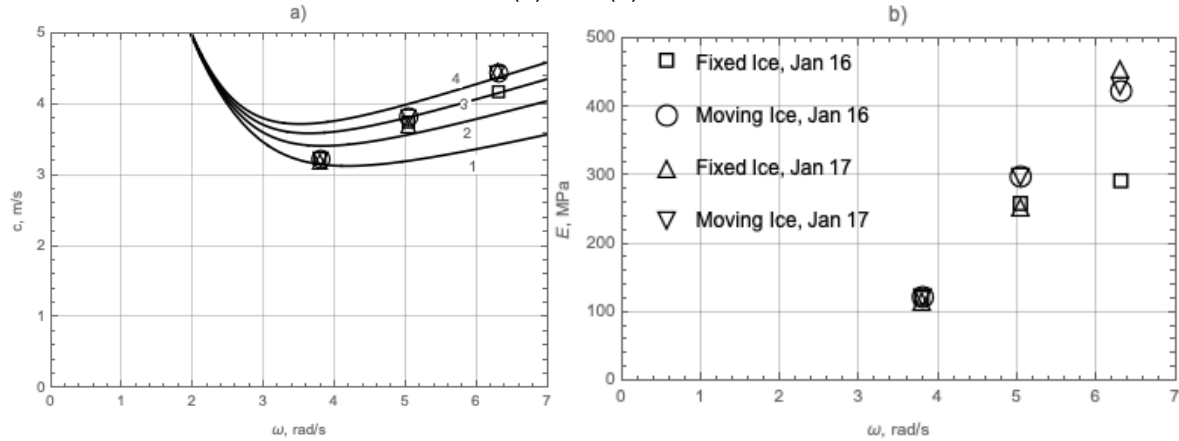


Figure 7. Wave speeds calculated from experimental data TGII (a). Lines 1, 2, 3, and 4 are constructed with elastic moduli of 100, 200, 300 and 400 MPa respectively. Elastic moduli of ice calculated from the experiment (b).

Figure 6b shows that the calculated values of ω and k are located within dispersion curves constructed with elastic moduli of 100, 200, 300 and 400 MPa. Figure 7a shows that the calculated wave speeds $c = \omega/k$ are close to the phase velocities of waves constructed with the same values of elastic modulus. Figure 7b shows that elastic moduli of ice calculated from the tests with wave frequency of 0.6 Hz, 0.8 Hz and 1 Hz are of about 100 MPa, 300 MPa and 400 MPa respectively.

5. INFLUENCE OF ICE CRACK ON WAVE DAMPING

The ice located in the tank with $x > 30 \text{ m}$ remained undestroyed in all tests. The first crack extending across the tank at the distance of 1-2 m from the ice edge and providing effective wave damping was discovered during TGII on January 17 in the next test after the tests described in the previous section. The crack was clearly visible from a distance, due to its cyclic opening and closing during wave propagation. Cycling pumping of the water or brine through the crack was also clearly visible (Fig. 8). It was not possible to locate crack at the bottom of the ice by manual inspection near the tank wall, while it was clearly visible at the upper ice surface.

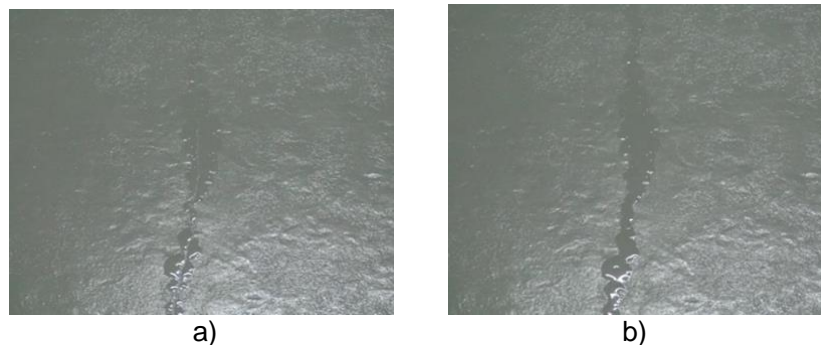


Figure 8. Photographs of (a) closed, and (b) open and brine-filled crack.

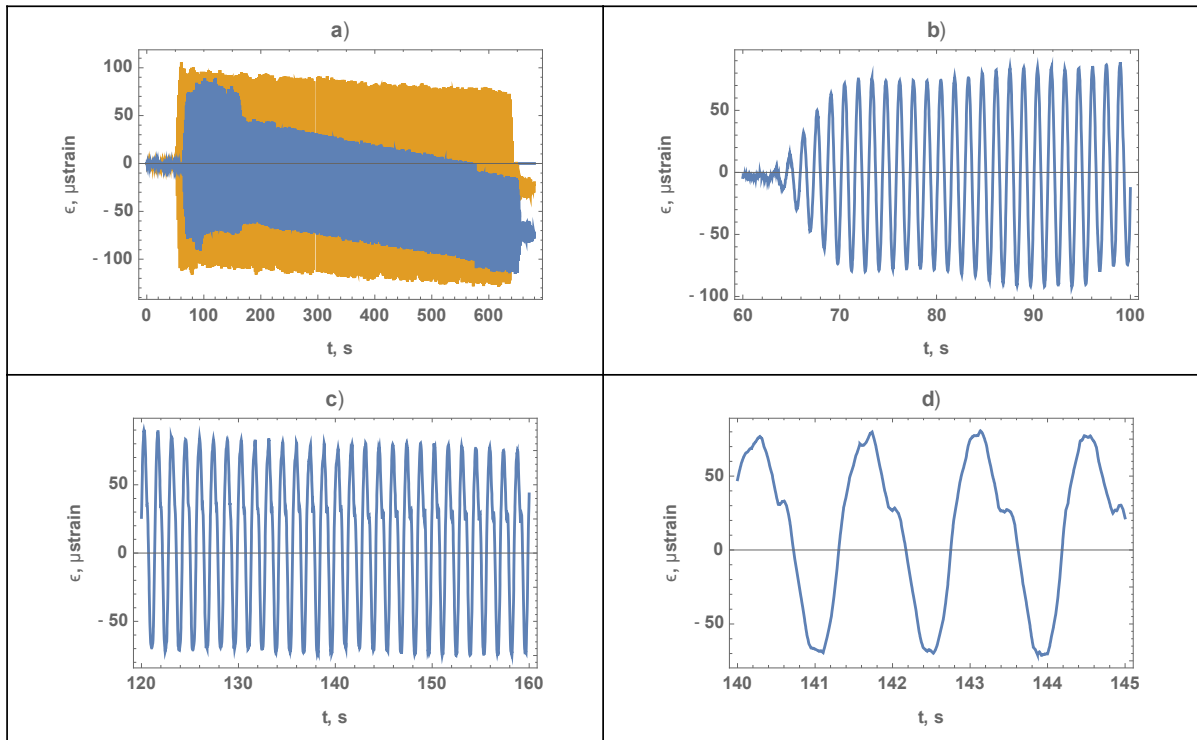


Figure 9. Strain records of FBGS1 in the test when the first crack was registered are shown by blue lines. Yellow line shows record of FBGS1 in the test before the crack formation.

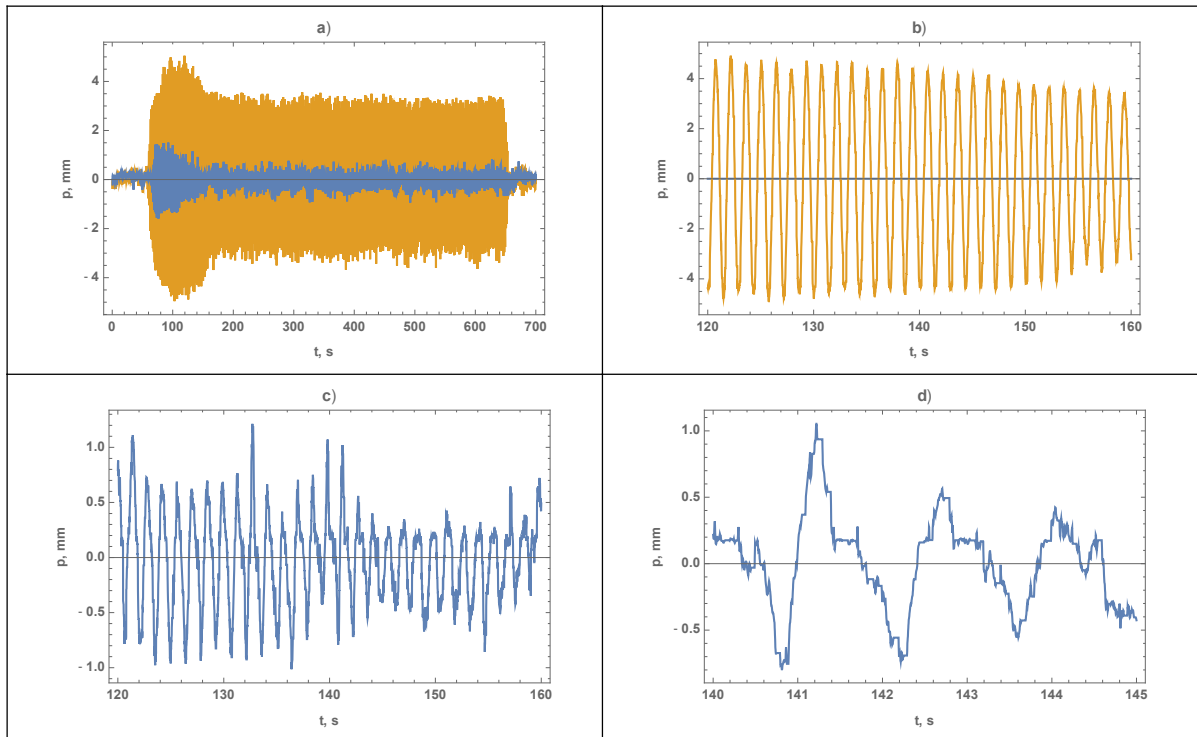


Figure 10. Strain records of pressure sensors WP1 (yellow lines) and WP3 (blue lines) in the test when the first crack was registered.

Figure 9 shows that the crack formation influenced the amplitude and shape of strains recorded by FBGS1. The strain amplitude became smaller in comparison with similar test performed before the crack formation (Fig. 9a). Strain signal changed from sinusoidal signal registered by $t < 120$ s (Fig. 9b) to the signal with two peaks in one wave period (Fig. 9c,d). Figure 10 shows the same effect registered by water pressure sensors WP1 and WP3 mounted on the tank wall at the depth

of 15 cm below the water (Fig.1). Sensor WP1 was mounted in ice free area near the wave maker, and sensor WP3 was mounted below the ice at the distance of about 12 m from the ice edge. Yellow line in Fig. 10a shows that wave amplitude created by wave maker in the beginning of the test was higher than in previous tests. It was probably the reason for the ice crack formation. Figure 10b shows that pressure record of WP1 has sinusoidal shape before and after the crack formation. Figure 10c shows a transformation of the pressure recorded by WP3 from sinusoidal signal to a signal with several maxima in one wave period. Pressure signals are not very smooth in comparison with FBGS signals because of the resolution of the pressure sensors.

6. INFLUENCE OF ICE MOTION ON WAVE DAMPING

Five markers from a Qualisys–Motion Capture System were used to record ice movements at 5 points. The data includes the records of the three coordinates of each marker as a function of time, with sampling frequency of 200 Hz. An example of the record of the ice motion along the tank in the test with moving ice is shown in Fig. 11a. Periods of the cyclic motion varied within 40–50 s. Representative speed of the cyclic motion is of 0.04 m/s.

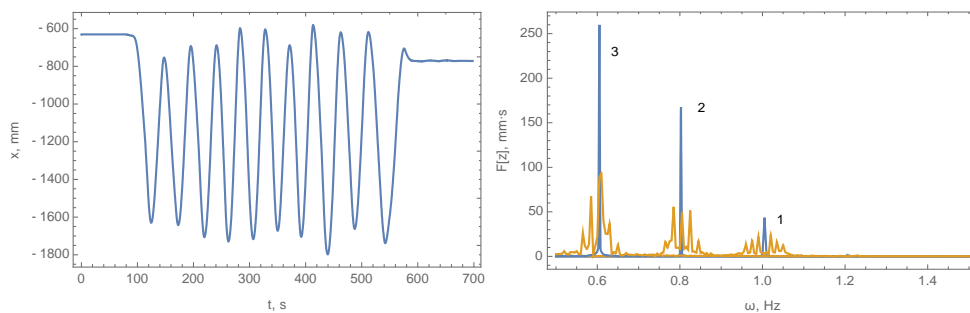


Figure 11. Records of the ice marker motion along the tank (left panel). Fourier spectrums of vertical oscillations of the ice in the tests (TGII) with fixed (blue lines) and moving (yellow) ice (right panel).

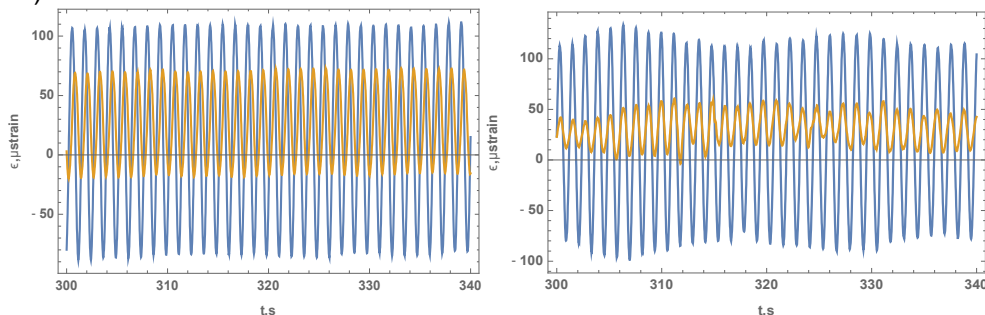


Figure 12. Examples of the records of FBGS1 (blue lines) and FBGS5 (yellow lines) in the tests (TGII) with fixed ice (left panel) and moving ice (right panel). Wave frequency is 0.8 Hz.

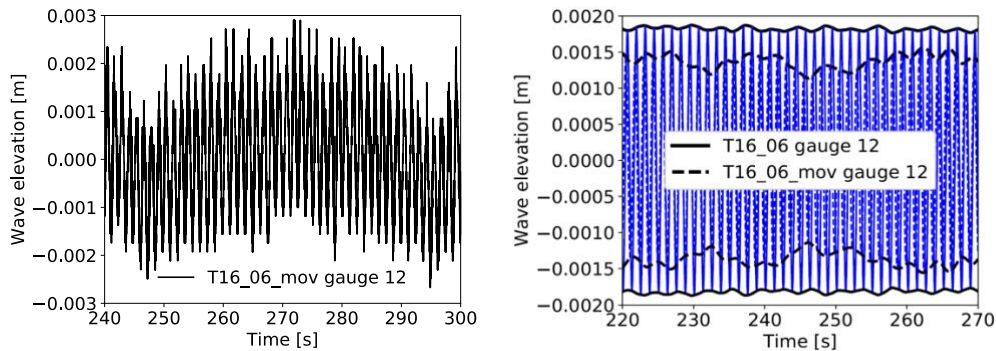


Figure 13. Wave modulation registered by US sensors in the test (TGII) with moving ice (left panel) and effect of wave modulation on the wave amplitude below the ice in the test with moving ice in comparison with the test with fixed ice (right panel). Wave frequency is 0.6 Hz.

Figures 11b, 12-14 show the influence of the ice motion on an increase of wave damping registered by different sensors. Yellow lines in Figure 11b show the decrease of spectral amplitude of the vertical motion of the ice and spectral spreading in the experiments with moving ice in comparison with the spectrum (blue lines) calculated from the experiments with fixed ice. Figure 12 shows the decrease of strain amplitudes recorded by FBGS sensors in the tests with moving ice in comparison with the strain amplitudes recorded in the tests with fixed ice. Figure 12b shows also the effect of low frequency wave modulations registered in the tests with moving ice. Figure 13 shows similar effects in the records of US sensors. Figure 14 shows the reduction of hits amplitudes recorded by AE sensors in the tests with moving ice in comparison with the hit amplitudes recorded in the tests with fixed ice.

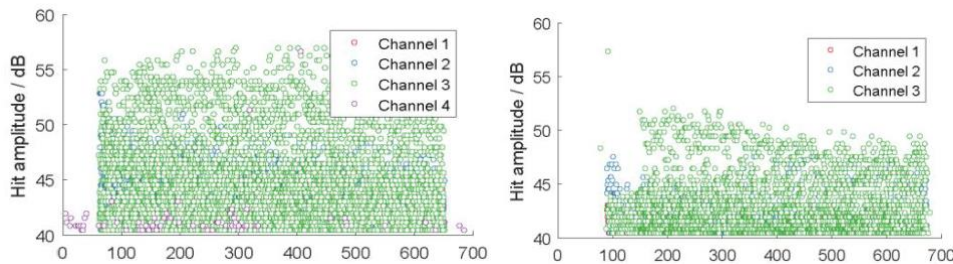


Figure 14. Hit amplitudes as a function of time, across three channels, for the tests (TGII) with fixed ice (left panel) and moving ice (right panel). Wave frequency is 0.8 Hz.

6. CONCLUSIONS

Analysis of wave speeds performed with FBGS sensors showed an increase of elastic modulus of ice with increasing of wave frequency in the tests of TGII with ice thickness of 5 cm. Calculated from the experiment dynamic value of elastic modulus varied from 100 MPa to 400 MPa when the wave frequency changed from 0.6 Hz to 1 Hz, while static value of elastic modulus measured by vertical displacements of ice loaded in the point was of around 250 MPa.

Several physical effects causing wave damping below the solid ice were observed in the experiments including perforation of the ice edge, formation of non-through cracks, ice break up by waves and under-ice turbulence generated by cyclic motion of the ice sheet along the ice tank. Not extended cracks, produced in the ice by waves, caused strong damping due to the cyclic pumping of the brine or water up and down through the ice. Wave damping in the region where the ice was broken by the waves and in the region with a net of non-through cracks prevented ice failure in the end of the tank in all experiments. Results from the Qualisys system, FBGS, US and AE sensors show stronger wave damping in experiments with moving ice. Thus, the experimental results confirm the importance of ice drift and under-ice turbulence for wave damping.

ACKNOWLEDGEMENT

The work described in this publication was supported by the European Community's Horizon 2020 Research and Innovation Programme through the grant to HYDRALAB-Plus, Contract no. 654110. The authors also wish to acknowledge the support of the Research Council of Norway through the PETROMAKS2 project Dynamics of floating ice and IntPart project Arctic Offshore and Coastal Engineering in Changing Climate. Authors of the paper thank HSVA staff for the help during the experiment, and Hayley Shen for the discussion of project proposals and experimental results.

REFERENCES

- Marchenko, A., Karulina, M., Karulin, E., Chistyakov, P., Sakharov, A., 2017. Flexural Strength of Ice Reconstructed from Field Tests with Cantilever Beams and Laboratory Tests with Beams and Disks. *Proceedings of the POAC17*, POAC17-177.
- Timco, G.W. and Weeks, W.F. (2010). A review of the engineering properties of sea ice. *Cold Regions Science and Technology*. 60, 107-129.